14 Other structures

14.1 Introduction

In this chapter, the wind loads on some structures not covered in Chapters 8 to 13, and appendages attached to buildings, will be considered. Some of these structures may be of lesser economic importance, but are often sensitive to wind loads, fail early during a severe windstorm and provide a source of flying debris.

In the following sections wind loads on free-standing walls (including noise barriers along freeways or motorways, and hoardings are discussed. Free-standing paraboloidal antennas for radio telescopes, and antennas of various geometries attached to towers or buildings, are considered. Wind loading of free-standing roofs or canopies, solar panels attached to the roofs of buildings, as well as appendages attached to buildings such as canopies, awnings and balconies, are also discussed.

14.2 Walls and hoardings

14.2.1 Single walls under normal and oblique winds

In Sections 4.3.1 and 4.3.2, the mean drag coefficients on walls on the ground are discussed in the context of bluff-body aerodynamics. Discussion of wind loads on free-standing walls under normal and oblique winds will be expanded in this chapter.

In Figure 14.1, mean and maximum net pressure difference coefficients acting on complete walls of various breadth/height ratios are shown plotted. These values are based on boundary-layer wind tunnel measurements (Letchford and Holmes, 1994) in open country terrain (Jensen numbers h/z_o in the range 50 to 160). The net pressure coefficient, C_{pn} is defined in equation (14.1) and, in this case, is equivalent to a drag coefficient.

$$C_{pn} = \frac{p_w - p_L}{\frac{1}{2}\rho_a \bar{U}_h^2} \tag{14.1}$$

where p_w is the area-averaged pressure coefficient on the windward face of the wall; p_L is the area-averaged pressure coefficient on the leeward face of the wall; and $\bar{U}_h$ is the mean wind speed at the top of the wall.

The maximum values were expected values for periods equivalent to 10 min in full scale. The mean net pressure coefficients show a small reduction in the range of b/h from 0.5 to 5 and, as previously shown in Figure 4.5. A larger reduction occurs for the maximum pressure coefficients – this is due to the reduction in spatial correlation for longer lengths of wall. About a 20% reduction in peak net load occurs as the wall length increases from one to four wall heights.

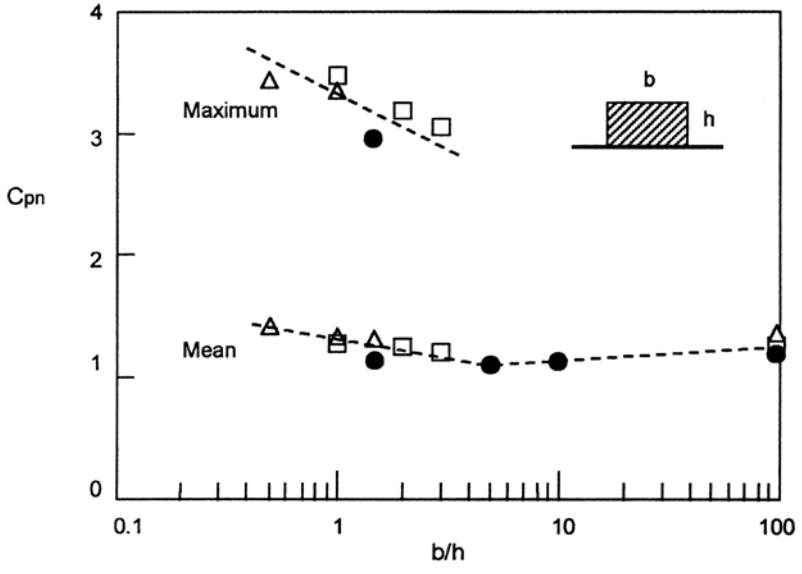

Figure 14.1 Mean and maximum pressure difference coefficients for free-standing walls (normal wind) (Letchford and Holmes, 1994).

For a wind direction at 45 degrees to the plane of the walls, the average net pressure coefficients are shown in Figure 14.2. In this case, the net mean pressure coefficient reaches a maximum for a *b*/*h* ratio of about 3 with lower values for longer walls. For this wind direction, there is a strong separation on the leeward face of the walls of this length ratio. For longer walls, re-attachment occurs and generates lower magnitude pressures on the leeward face.

For mean wind directions normal to the wall, the net pressures do not vary much along the length of the wall. However, this is not the case for the oblique wind direction. Figure 14.3 shows how the mean net pressure coefficient varies along the wall length. The flow separation behind the windward edge generates very high pressures for the first one to two wall heights from the windward edge. This also occurs for elevated hoardings (Figure 4.8 and Section 14.2.4), and is usually the critical design case for wind loads.

14.2.2 Walls with corners

The effect of a right-angled corner at a free end of a wall for various wind directions on mean pressure coefficients averaged over a vertical line, distant *y* from the corner, are shown in Figures 14.4 and 14.5.

For a wind direction of 0 degrees, with the corner running downwind, the effect is small; however for 180 degrees there is an increase in mean pressure coefficient of up to 30% (Figure 14.4). However, for the 45 degree wind direction (i.e. blowing from outside the corner), there is a significant reduction in mean pressure coefficients, for the region immediately adjacent to the corner (Figure 14.5).

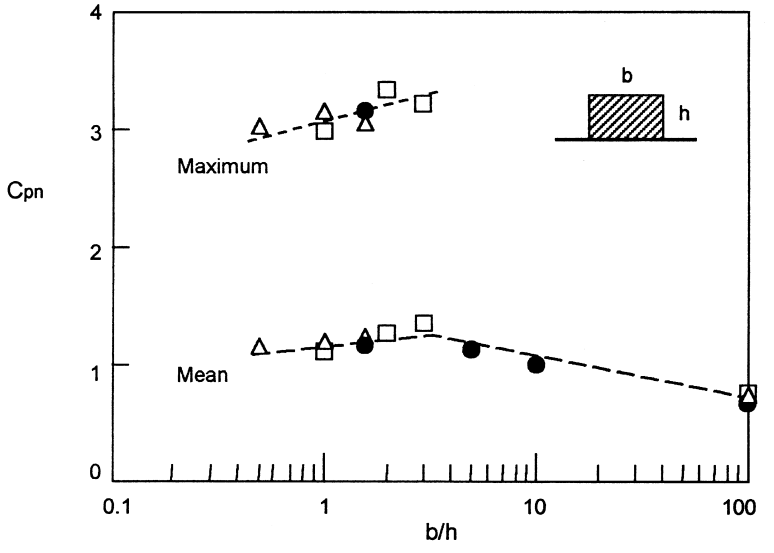

Figure 14.2 Mean and maximum pressure difference coefficients for free-standing walls (oblique wind) (Letchford and Holmes, 1994).

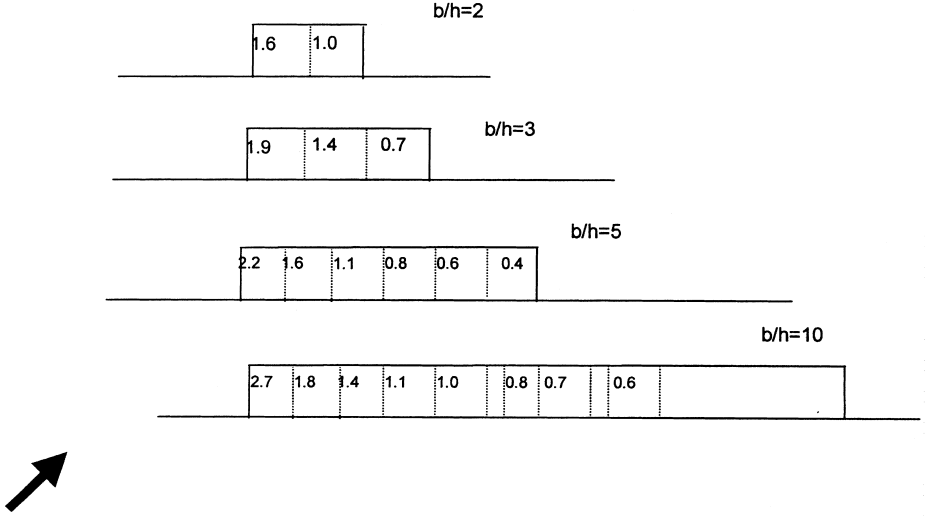

Figure 14.3 Mean pressure difference coefficients for free-standing walls (oblique wind).

14.2.3 Parallel two-dimensional walls

There is an increasing tendency to provide noise barriers along freeways and motorways when they pass through urban areas. These are generally parallel walls spaced at the width of the roadway, so that shielding effects from the opposite wall may be important for certain wind directions. The wind loads on these walls are also affected by other disturbances to the wind flow, such as topographic features and elevated bridges.

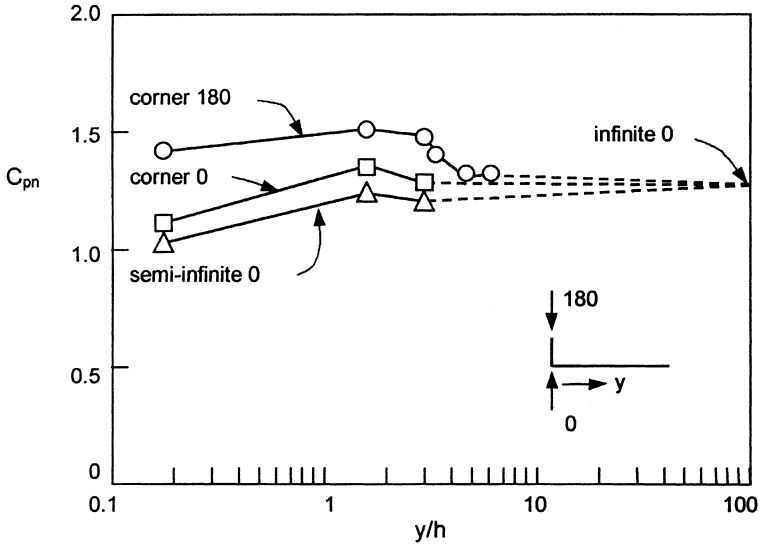

Figure 14.4 Mean pressure difference coefficients for free-standing walls with corners (normal winds) (Letchford and Holmes, 1994).

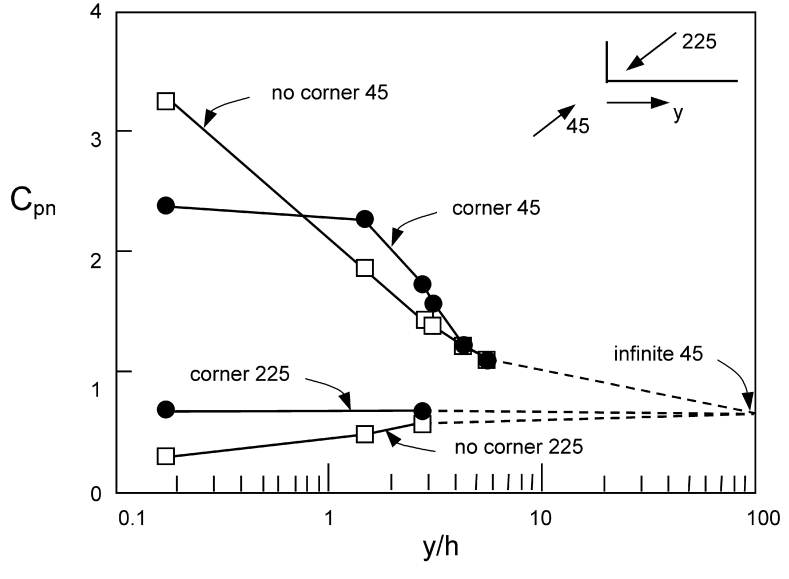

Figure 14.5 Mean pressure difference coefficients for free-standing walls with corners (oblique winds) (Letchford and Holmes, 1994).

Figure 14.6 shows the variation of mean, r.m.s., maximum and minimum net pressure coefficients on one wall of a pair of parallel ones, for various spacings. The pressure coefficients are based on the mean wind speed at wall height in the undisturbed flow. A negative value of wall spacing/wall height means the second wall is *downwind*. These measurements were carried out in simulated atmospheric boundary-layer flow in a wind tunnel. The values of Jensen number, h/z_o, (Section 4.2.3) for the wall heights used in the tests were about 10 to 20.

The pressure tappings were arranged in vertical rows, with spacings chosen that the pressures averaged together as a group of four (Section 7.5.2), gave a measure of the bending moment at the base of the wall. Thus the measurements are of base moment coefficients defined as:

$$C_M = \frac{M}{\frac{1}{4}\rho_a \bar{U}^2 h^2} \tag{14.2}$$

where M is the moment about the base, per unit length of wall. This is also an effective net pressure coefficient which, when applied uniformly over the well height, will give the correct base moment. Averaging of peak and fluctuating pressures was carried out over one wall height horizontally along the wall axis.

The mean pressure difference is negative when the upwind wall is about two wall heights away from the shielded wall; that is, it acts *upwind*. Small shielding effects are felt when the upwind wall is as much as 20 wall heights upwind.

Figure 14.7 compares the mean, maximum and r.m.s. net effective pressure coefficients for the windward wall of the pair of parallel walls on a bridge with two different values of clear space underneath (Holmes, 2000). The thickness of the bridge deck was equal to the wall height. Values are for s/h equal to 0, 2 and 4, where s is the clear spacing under the bridge. All pressure coefficients are calculated with respect to the mean wind speed at the height of the top of the wall ($s + 2h$) in the undisturbed flow.

Figure 14.7 shows there is little difference between the net pressure coefficients for the cases of s/h equal to 2 or 4, when there is airflow beneath the bridge. However, when s/h is equal to 0 – that is the 'bridge' forms a flat-topped cliff, the mean and maximum net pressure coefficients are about 90% of the values on the elevated bridges; the r.m.s. pressures are about 80% of those in the elevated case.

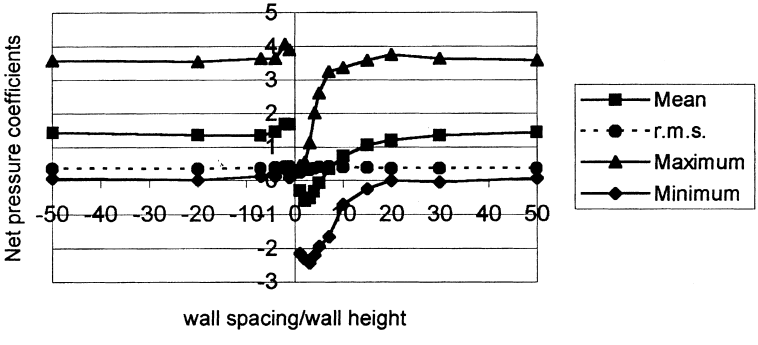

Figure 14.6 Parallel walls on flat level ground – effect of wall spacing (Holmes, 2000).

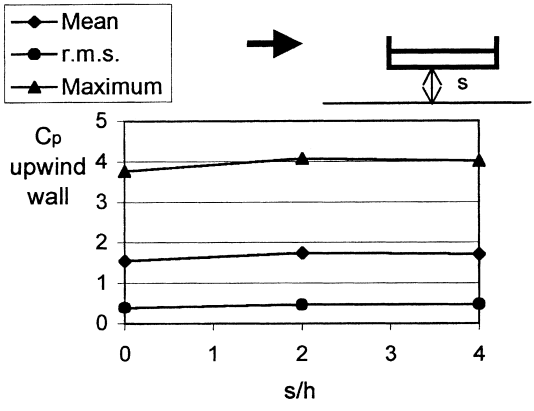

Figure 14.7 Effect of clear space, *s*, for parallel walls on bridges (Holmes, 2000).

14.2.4 Elevated hoardings

The net wind pressure coefficients on elevated hoardings have generally similar characteristics to those on free-standing walls. The effect of elevation is to increase the magnitude of the net pressure coefficient for winds normal to the surface. The average mean pressure coefficient depends on the spacing to the ground beneath the hoarding. For a spacing equal to the depth of the hoarding, a mean net pressure coefficient (with reference to the mean velocity at the top of the hoarding), of about 1.5 occurs.

The oblique wind direction can produce large pressure differences near the windward end, as for free-standing walls (Figure 4.8).

Design data for elevated hoardings and signboards is given in both the Australian (Standards Australia, 1989) and British Standards (B.S.I., 1997).

14.3 Free-standing roofs and canopies

Free-standing, or 'canopy' roofs, without walls, are often used for basic shelter structures – such as those at motor vehicle service stations and railway stations, or for coverage of industrial, mineral or agricultural products. The wind loads on roofs of this type attached to buildings are discussed in Section 14.4.1.

Free-standing roofs which are completely free of stored material underneath, allow air to flow freely underneath; this generally results in negative, or near zero, underside pressures with respect to atmospheric pressure. The addition of stored material underneath the roof in sufficient quantity will cause full or partial stagnation of the airflow, and positive pressures underneath. The nature of the upper surface pressures depends on the roof pitch and the wind direction.

Wind pressure coefficients on free-standing roofs are usually quoted in the form of net pressure coefficients, as defined in equation (14.1). The pressures can normally be assumed to act normal to the roof surface. The usual sign convention is that positive net pressures act downwards. This sign convention and the most common three types of free-standing roof geometry are shown in Figure 14.8.

Although the pressures normal to the roof surface are the dominant ones, frictional forces acting parallel to the roof surfaces, can also be significant, and it may be necessary to consider them, when designing the bracing required to resist horizontal forces.

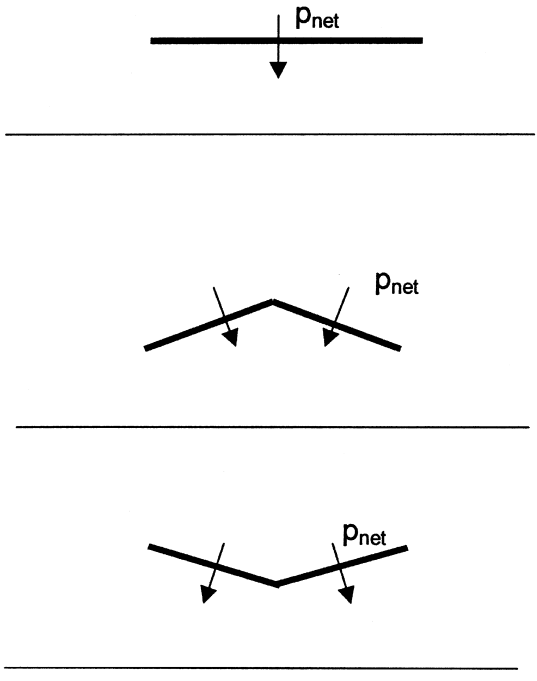

Figure 14.8 Types of free-standing roof, and sign convention for net pressures.

Free-standing roofs have been studied in both wind-tunnel tests (Gumley, 1984; Letchford and Ginger, 1992; Ginger and Letchford, 1994), and full-scale experiments (Robertson *et al.*, 1985).

Net pressure coefficients along the centre line of a free-standing 'Dutch barn' with 15 degrees roof pitch, measured in full scale (Robertson *et al.*, 1985) are shown in Figure 14.9. The roof is completely empty underneath. Positive (downwards) pressure differences exist over the windward quarter of the roof for all wind directions. The largest negative loads occur near the middle of the roof for a wind direction normal to the ridge.

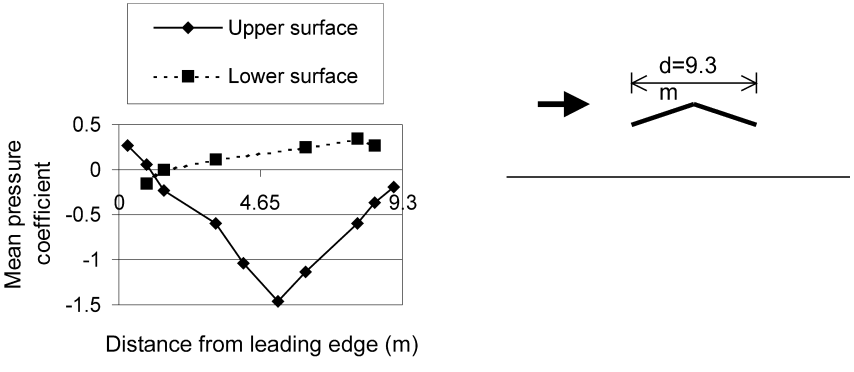

Figure 14.9 Mean pressure coefficients along the centre line of a free-standing roof with 15 degree pitch (Robertson *et al.*, 1985).

Letchford and Ginger (1992; Ginger and Letchford, 1994) carried out extensive wind tunnel measurements on pitched free roofs (empty under) of approximately square plan, with a range of pitches up to 30 degrees. Mean and fluctuating pressure measurements from single points and area-averaged (Section 7.5.2) over six panels, were made. In addition, correlation coefficients (Section 3.3.5) were measured for the six panel pressures enabling fluctuating total forces (Section 4.6.6), and equivalent static loading distributions to be derived (Section 5.4.3).

Mean area-averaged net pressure coefficients for half the pitched roof are shown in Figure 14.10. For the 0 degree wind direction, the half roof is on the windward side. Figure 14.10 shows that significant positive pressures (for wind directions of 0 to 30 degrees) and negative pressures (for wind directions of 120 to 180 degrees), occur for roof pitches of 22.5 and 30 degrees. For roof pitches of 15 degrees or less, the net pressure difference coefficients are not large for any wind direction.

The peak (maximum and minimum) area-averaged pressure difference coefficients generally showed similar behaviour to the mean coefficients shown in Figure 14.10, with the 22.5 degree and 30 degree pitch roofs clearly showing larger magnitudes. When peak total uplift and horizontal forces were calculated, substantial reductions of up to 50% from values calculated from the non-simultaneous peaks on windward and leeward halves, were obtained, due to the poor correlation between fluctuating wind pressures on the two surfaces (Ginger and Letchford, 1994).

Appendix F gives an example of the calculation of maximum and minimum lift and drag on a pitched free roof, and the effective static pressures producing them, based on data from Ginger and Letchford (1994).

14.4 Attachments to buildings

14.4.1 Canopies, awnings and parapets

Several configurations of horizontal canopy attached to one wall of a low-rise building have been investigated (Jancauskas and Holmes, 1985). The width of the canopy and the

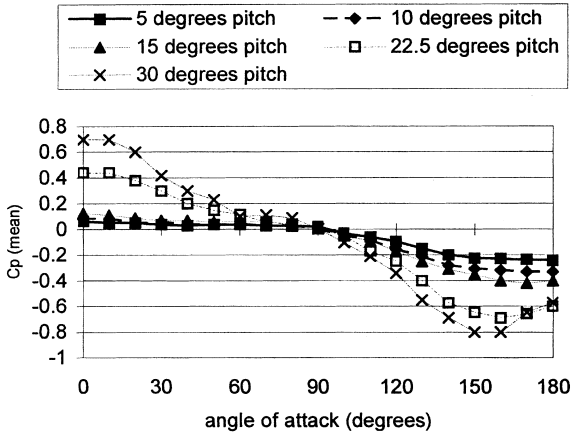

Figure 14.10 Mean pressure difference coefficients for pitched free roofs, averaged over a half roof (Letchford and Ginger, 1992).

height of the canopy position on the wall were the variables that were investigated. A narrow canopy mounted at the top of the wall behaves similarly to eaves on the roof.

For wind directions normal to the adjacent wall, the peak net force across the canopy is strongly dependent on the non-dimensional ratios, h_c/h, and h_c/w_c. h_c is the height of the canopy above the ground, h is the total height of the adjacent wall, and w_c is the width of the canopy.

For the peak vertical uplift force coefficient, $\hat{C}_Z$, based on the mean wind speed at the height of the canopy, the following conservative relationships were proposed, based on the wind-tunnel measurements:

$$\text{for } \frac{h}{h_c} = 1.0,\ \hat{C}_Z = 1.0 + 1.3(h_c/w_c) \text{ or } 4.0, \text{ whichever is the lesser}$$

$$\text{for } \frac{h}{h_c} = 0.75,\ \hat{C}_Z = 1.0 + 0.4(h_c/w_c) \text{ or } 4.0, \text{ whichever is the lesser}$$

$$\text{for } \frac{h}{h_c} = 0.5,\ \hat{C}_Z = 1.0 \tag{14.3}$$

where,

$$C_Z = \frac{F_z}{\frac{1}{2}\rho_a \bar{U}_c^2 A}$$

F_z is the net vertical force on the canopy (positive upwards); $\bar{U}_c$ is the mean wind speed at the canopy height; A is the plan area of the canopy.

Equation (14.3) can be applied to canopies with pitch angles within five degrees of the horizontal. Appropriate adjustment is required if it is applied with gust wind speeds; such adjustment has been made for the rule incorporated in the Australian wind loading standard (Standards Australia, 1989).

The relationships of equation (14.3) are compared with the experimental data in Figure 14.11.

The higher values obtained for canopies or awnings near the top of the wall (or eaves), can be explained by the high flow velocities occurring on the upper side of the canopy producing significant negative pressures; on the underside of the canopy, stagnation and hence positive pressures occur. When the canopy is mounted part-way up the wall, stagnation of the flow occurs on the wall, both above and below the canopy. In this situation, the mean net force coefficients are low, but turbulence produces finite peak loads in both directions.

Parapets, and their effect on roof pressures on flat roofs, have been the subject of several wind tunnel studies. In the early work there were some conflicting conclusions drawn by different laboratories, but the issue was largely resolved using large models and a high density of pressure tappings (Kind, 1988). With or without parapets, the worst suction peaks occur in small zones near the upwind corner of the roof, for wind directions nearly bisecting the corner. The worst suction coefficients decrease monotonically with increasing relative parapet height. The amount of the reduction depends also on the height/width ratio of the building to which the parapet is attached.

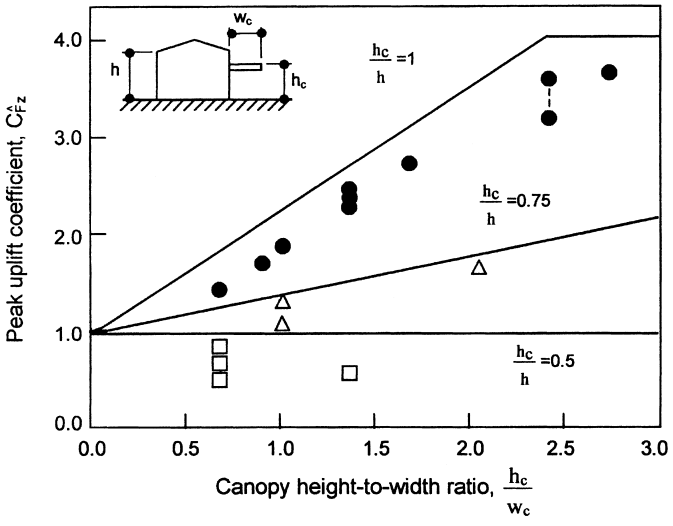

Figure 14.11 Peak uplift force coefficients for attached canopies (Jancauskas and Holmes, 1985).

14.4.2 Solar panels on roofs

The wind loads on solar panels attached to the roofs of a building are closely related to the flow over the roofs of the building itself, since the latter is a much larger bluff body. Figure 14.12 shows the various geometric variables that are significant in determining the wind loads on solar collector panels on a pitched roof building (Tieleman *et al.*, 1980).

The following summarizes the effects of the various solar panel and building variables on wind loads:

- 'Stand-off' spacing from the roof, *d*, – increasing stand-off appears to reduce net

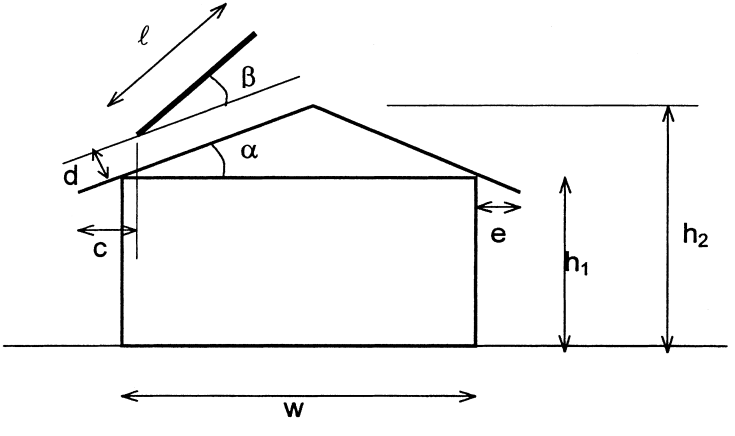

Figure 14.12 The variables affecting wind loads on solar panels (Tieleman *et al.*, 1980).

uplift load (normal to roof), but increases the wind force acting on the panel parallel to the roof (Newton, 1983).
- Module shape and size – the combined peak load on a row of panels is significantly less than that on a single panel, due to area reduction effects on the fluctuating pressures.
- Roof pitch – higher roof pitch produces lower uplift loads, but increasing downwards wind loads (as for the loads on the roofs of low-rise buildings generally).
- Proximity to eaves – the end panel (adjacent to the eaves) experiences considerably higher loads than the interior panel in a row.
- Wind direction – the worst uplifts occur for oblique wind directions to a row of collector panels.
- Roof height – the pressure *coefficients* for panels on two-storey buildings are lower than the equivalent values for single-storey buildings.

To optimize the upwards wind loading on solar panels, it is clearly a good idea to increase the stand-off clearance, as this reduces the net uplift. Increasing the angle β, so that the inclination of the panel is greater than that of the roof pitch, would appear to increase wind loads. It is better to locate panels away from the roof edges (eaves and ridges), and the uplift loads for parallel-mounted panels ($\beta = 0$) are lower for higher pitch roofs.

14.5 Antennas

14.5.1 Radio telescopes

Wind loads on the antennas of large steerable radio telescopes – usually with dish reflectors of paraboloidal shape – are of critical importance for several design criteria (Wyatt, 1964):

- Overall strength for safety in extreme winds
- Loads on drive system
- Freedom from oscillations
- Pointing accuracy
- Distortion of the reflector

The last four of the above conditions are serviceability criteria. Very small tolerances are required for the operation of these antennas.

The main source of wind loads is the paraboloidal dish itself. If the dish is impermeable, the pressures acting on it may be assumed to act normal to the surface, with negligible contributions from skin friction. For a paraboloid, the normal to any point on the surface passes through the generating axis, at a point $2f$ measured along the axis from that point, where f is the focal length. Therefore, it may be assumed, that the resultant aerodynamic force will act through a point on the axis, distant from the vertex by $2f$ plus half the depth of the dish, d (Wyatt, 1964).

Considering first the case with the wind direction normal to the altitude axis of rotation of the dish as shown in Figure 14.13. Resolving the aerodynamic forces in body axes (Section 4.2.2), the force coefficients are given by:

$$C_X = \frac{F_x}{\frac{1}{2}\rho_a \bar{U}_h^2 A} \tag{14.4}$$

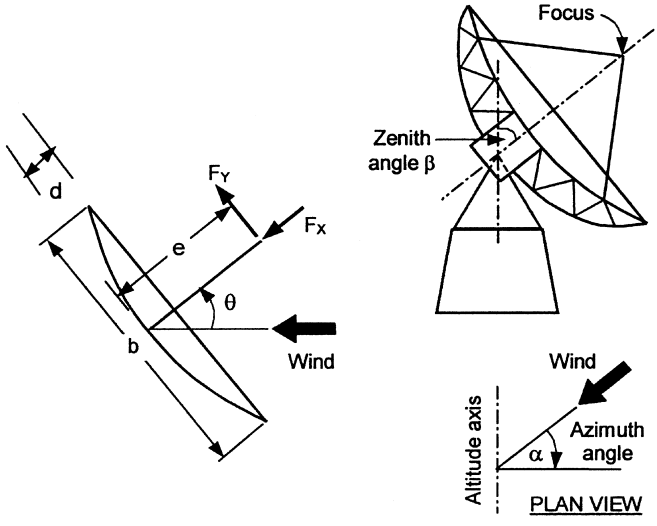

Figure 14.13 Resultant aerodynamic forces on the dish antenna of a radio telescope (Wyatt, 1964).

$$C_Y = \frac{F_Y}{\frac{1}{2}\rho_a \bar{U}_h^2 A} \tag{14.5}$$

where A is the projected area normal to the dish, given by $\pi\frac{b^2}{4}$.

Following the arguments in the previous paragraph, the eccentricity, e, of the aerodynamic force can be closely approximated by (Wyatt, 1964):

$$e = 2f + \frac{d}{2} = 2f\left[1 + \left(\frac{b}{8f}\right)^2\right] \tag{14.6}$$

Tests in smooth uniform flow (Wyatt, 1964) indicate maximum values of C_x of about 1.7 when the angle of attack, α, is about 45 degrees. The transverse force coefficient C_Y is approximately constant with f/b when expressed in the form $(f/b)C_Y$, with a maximum value of about 0.05, for α equal to about 135 degrees. The transverse force F_Y generates a moment about the vertex equal to $F_Y.e$.

It is found that the effect of a boundary-layer mean wind profile has a relatively small effect for wind directions facing the wind. However, the effect is greater when the wind is blowing obliquely on to the rear of the paraboloid. As shown in Figure 14.14, the effect is to increase the moment about the altitude axis and decrease it about the azimuth axis (Wyatt, 1964).

In Figure 14.14, the moment coefficients are defined as follows:

$$C_M = \frac{M}{\frac{1}{2}\rho_a \bar{U}_h^2 A b} \tag{14.7}$$

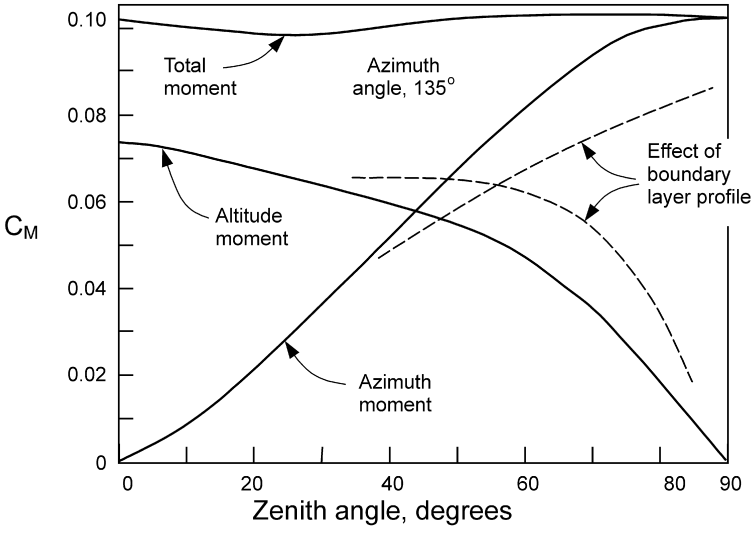

Figure 14.14 The effect of velocity profile on the aerodynamic moments on a radio telescope (Wyatt, 1964).

14.5.2 Microwave dish antennas

The drag forces acting on small dish antennas used for microwave frequency transmission, are of interest for the structural design of the towers supporting them. In the past, total drag forces for tower design have been obtained by simply adding the drag measured on the antennas in isolation to that determined for the tower without antennas. This will overestimate the total drag in many cases, as usually the antennas will shield part of the tower, or vice-versa; also the drag on an antenna itself in the presence of the tower will be different to that on the antenna in isolation.

Figure 14.15 shows the drag coefficient for an impermeable unshrouded dish obtained as a function of the wind incidence angle measured from the normal to the plane of the dish, measured in both smooth (approximately 1% turbulence intensity), and turbulent flow (10% turbulence intensity) (Holmes *et al.*, 1993). The reference area is the projected area of the dish, $\pi\frac{b^2}{4}$.

The drag coefficient for the isolated dish is maximum with a wind direction normal to the plane of the dish, but does not reduce much in an angular window within 30 degrees to the normal. The maximum drag coefficient, based on the disc area is about 1.4. A large reduction occurs for wind directions from 40 to 80 degrees to the normal. The effect of turbulence intensity is small.

The concept of *interference factor* is illustrated in Figure 14.16. The drag of an isolated antenna should be multiplied by this factor to give the measured incremental contribution to the total tower drag. The sum of the drag on the tower segment, D_t, and the incremental contribution from the antenna, $K_i D_a$, gives a total effective drag, D_e.

The interference factor for a single dish attached to a face of a lattice tower, with square cross-section and a solidity ratio of 0.3, is shown graphically, as a function of wind direction, θ, relative to the tower face in Figure 14.17 (Holmes *et al.*, 1993). The maximum interference factor of about 1.3 occurs at wind directions for which the dish accelerated

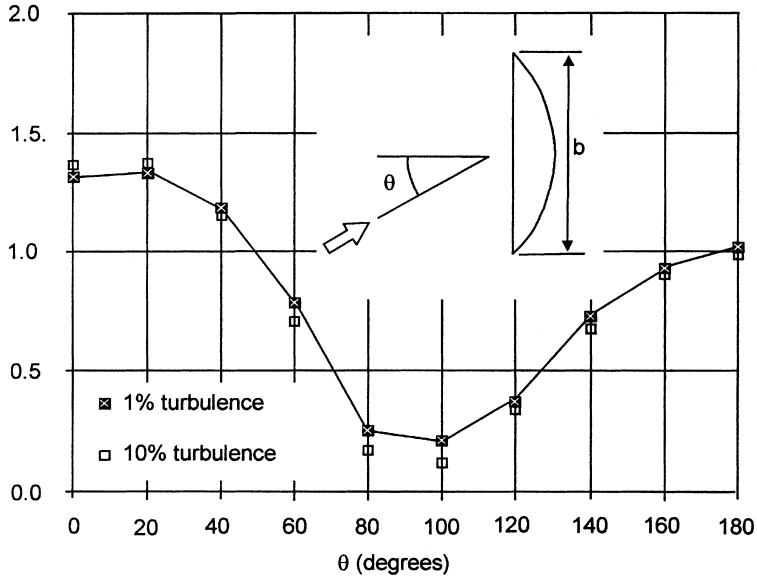

Figure 14.15 Drag coefficient as a function of angle of attack for an isolated dish antenna (Holmes *et al*., 1993).

the airflow over the tower, i.e. for wind directions of 90 and 270 degrees. For wind directions of 0 and 180 degrees, where mutual shielding occurs, interference factors as low as 0.5 can occur.

An empirical form for the interference factor, K_i, based only on the solidity and drag coefficient of the tower which fits the experimental data in Figure 14.17, and data from other cases, takes the form:

$$K_i = \exp[-k(C_D\delta)^2].[(1+t) + t\cos 2(\theta - \theta_d - 90^\circ] \tag{14.8}$$

where C_D is the drag coefficient for the tower or mast section alone, based on the projected area of members in one face, measured normal to the face; δ is the solidity of a face of the tower; k is a parameter equal to 1.2 for a square tower (E.S.D.U., 1981); t is an adjustable parameter (equal to 0.5 in Figure 14.17); θ_d is the angle of the normal to the dish antenna relative to the tower.

As well as drag (along-wind) forces, there may be significant cross-wind forces acting for wind directions parallel, or nearly parallel, to the plane of a solid dish. These should be taken account of when designing support attachments for the dish. Basic aerodynamic force coefficients are often obtainable from the antenna manufacturers, although these would not generally include interference effects.

14.5.3 Rotating radar antennas

Aerodynamic loads on large rotating radar antennas, such as those used at large airports, pose a particular serviceability problem due to the variations in torque that arise. The operation of the antennas imposes strict limits on variations in angular velocity, and this

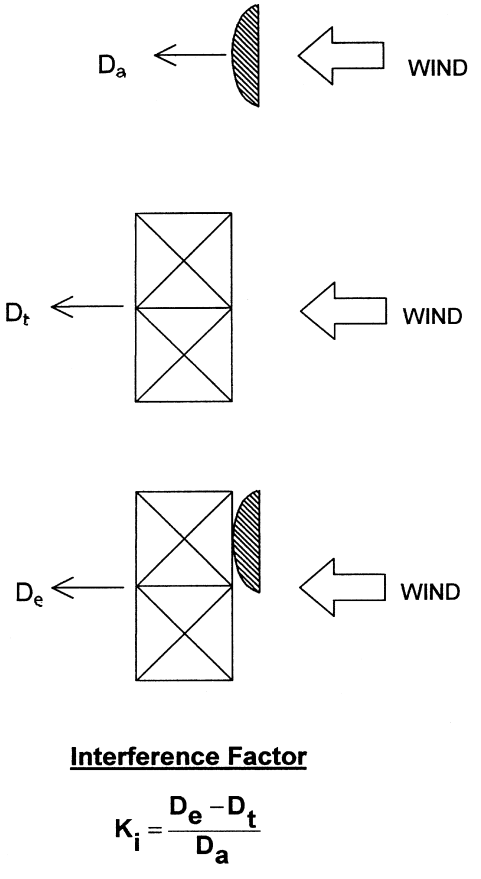

Figure 14.16 Concept of interference factor for incremental antenna drag.

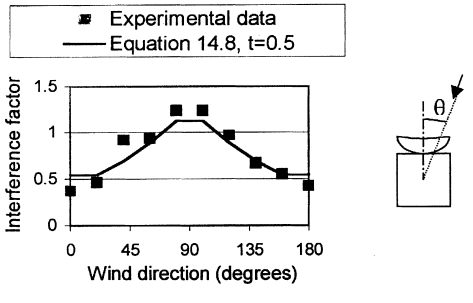

Figure 14.17 Interference factor as a function of wind direction for a single microwave dish added to a square lattice tower (Holmes *et al.*, 1993).

in turn limits the variations in torque that the drive motor must overcome. Wind-induced variations in torque arise from two sources:

- Variations in the azimuth angle between the wind direction and the antenna
- Horizontal wind turbulence

At the rates of rotation used in practice, the first source of aerodynamic torque variation appears to be dominant.

The effect of rotation of the antenna can be treated by a quasi-steady approach. This results in the predicted variation of torque being obtained from static tests in a wind tunnel, in which the azimuth angle is varied. The effect of rotation is assumed to result in a static shift in the fluctuating torque curve obtained from such tests (Sachs, 1978; Lombardi, 1989). However the quasi-steady theory has been found to be only approximately correct at high rotational speeds (Lombardi, 1991).

The use of small fins on the back of the antenna has been found to be effective in reducing the aerodynamic torque. These are small lifting surfaces which produce a counteracting torque. Figure 14.18 shows measured torque coefficients obtained from a rotating wind tunnel model with and without fins (Lombardi, 1991).

Unfortunately all the wind tunnel measurements on rotating radar antenna have been carried out in smooth uniform flow. The effect of turbulent boundary-layer flow is uncertain, but the most likely effect is to smooth out the torque versus yaw angle graphs, such as those shown in Figure 14.18.

14.5.4 Mobile telephone antennas

Antennas for mobile telephone cells typically consist of several radiating antennas within fibreglass or plastic radomes, mounted on poles or towers, which may in turn be mounted above buildings or other structures. By their nature they are in exposed positions, and thus the interference, or shelter, effects from other structures is usually small. However the mutual aerodynamic interference between radomes can be considerable.

Many of these antennas have been tested at full scale in large wind tunnels, for aerody-

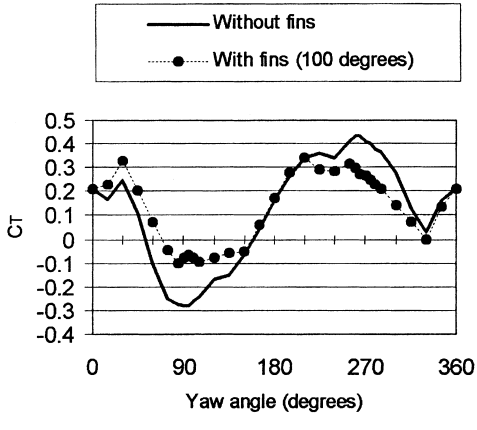

Figure 14.18 Aerodynamic torque coefficient versus yaw angle for rotating radar antennas (Lombardi, 1991).

namic force coefficients, but the data are usually proprietary in nature, and not freely available. The force coefficients have been found to be dependent on Reynolds number, so that model testing at small scales will produce unreliable results. However drag coefficients at high Reynolds number from full-scale measurements, typical of these antenna elements, which illustrate the mutual interference effects are shown in Figure 14.19.

The drag coefficient for wind normal to the curved face of an antenna is around 1.1 based on the projected frontal area. This value is reduced for wind directions in which the frontal area presented to the wind is reduced, as illustrated for the value shown for a wind direction 120 degrees from the normal.

When the antenna elements are grouped in threes, the combined drag coefficient (based on the frontal area of *one* radome element) is greatly reduced. As shown in Figure 14.19, the effect of the two downwind elements in the widely spaced (left side) cluster is neutral – i.e. the drag of the upwind element in isolation is the same as the combined drag of the group of three. For the closely spaced cluster, which resembles a single bluff body with curved surfaces, the overall drag is more than 20% less than that of the upwind radome in isolation.

Sometimes up to nine antennas are grouped together on a triangular frame, as shown in Figure 14.20. For the case shown, the antennas on a single face are well separated to avoid large aerodynamic interference effects, but those at the corners may experience slight increases in drag due to mutual interference (Section 4.3.1, and Marchman and Werme, 1982). The six downwind antennas are shielded both by the upwind antennas, and by the supporting pole. Full-scale wind tunnel tests on complete antenna headframes indicate an overall reduction of about 30% in the combined drag is obtained, when comparing the combined drag of the group, with that obtained by the summation of contributions from individual elements.

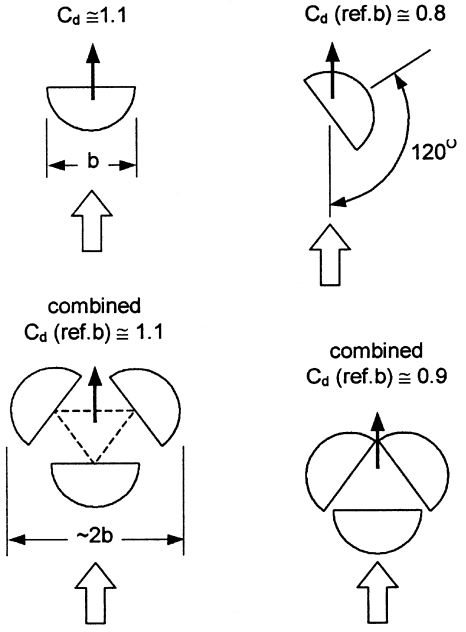

Figure 14.19 Typical drag force coefficients for mobile telephone antenna elements.

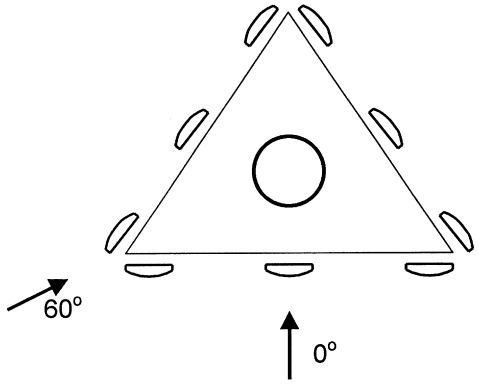

Figure 14.20 A group of mobile telephone antenna elements on a triangular frame.

Isolated radome elements will also experience cross-wind forces at oblique wind directions. However these will be largely cancelled by opposite forces from other elements, when they are part of a group.

14.5.5 UHF antennas

Antennas for the transmission of ultra-high frequency television broadcasting signals (including digital television), consist of fibreglass or plastic radomes mounted on four or five-sided masts, and are usually quite 'solid' cross-sections. They are of the order of 1 m in breadth, and about 20 m long. They are usually mounted at the top of free-standing or guyed towers.

The drag coefficient for these cross-sections depends on the porosity of the cross-section – i.e. the ability of the wake to be vented to the windward side. Measurements on full-size antenna sections have yielded drag coefficients in the range of 1.1 to 1.6, with some dependency on wind direction.

UHF antennas have experienced significant cross-wind response due to vortex shedding (Sections 4.6.3 and 11.5). This has often occurred for antennas on guyed masts, which have a lower damping than free-standing lattice towers. Such responses occur at a critical velocity, that is quite low, and in atmospheric conditions with low turbulence intensities. The prediction of cross-wind response due to vortex-shedding for *circular* cross-sections was discussed in Section 11.5. Methods also exist for *non-circular* cross-sections (e.g. E.S.D.U., 1990). These methods require information on the Strouhal number (rate of vortex shedding – see Section 4.6.3), and fluctuating cross-wind force coefficients (Section 4.6.4). These would not be well-defined for the complex cross-sections of UHF antennas.

If vibrations occur they can be mitigated by the use of simple damping devices, such as liquid dampers (Section 9.9.4), or *hanging chain* dampers (Koss and Melbourne, 1995).

14.6 Lighting frames and luminaires

Street lighting, flood lighting for railway yards, sporting grounds and industrial areas, are bluff bodies of a variety of shapes and porosities. There are considerable interference effects when luminaires are arranged in groups. As for antennas, the drag of many types

has been measured in wind tunnels, but is usually commercially sponsored, and the results are not readily obtainable.

The largest drag coefficients of single lights for any wind direction fall in the range of 1.0 to 1.5, based on the largest frontal area projected vertically. The lower value applies to the more rounded types, and the higher value to sharp-edged lights.

Large rectangular headframes, with many luminaires attached, such as large floodlight systems for sporting grounds, may be treated as porous flat plates (see Section 4.3.1). A value of drag coefficient of 1.5, based on the projected 'solid' or 'wind' area is an appropriate one for solidities of 0.3 to 0.7.

The wind loads on supporting poles for lighting are discussed in Chapter 11.

14.7 Industrial complexes and offshore platforms

Estimation of wind loads for elements of industrial complexes such as power stations, petroleum refineries, or mineral processing plants, is an extremely difficult problem. Such complexes consist of a large number of closely spaced bluff bodies, with considerable aerodynamic interference between them. It would normally be extremely conservative to estimate the total wind drag force by summing up the contributions from individual elements, as if they were isolated bluff bodies, although this is often done. The complexity and unique layouts of these plants means that is difficult or impossible to give general rules for estimating wind forces, except for some relatively common situations such as closely spaced circular cylinders. One useful approach, which avoids gross overestimation of drag forces, is to treat a closely spaced complex of bodies in a 'global' way as a single 'porous' bluff body, for which data are readily available.

Offshore platforms, used for oil exploration and production, are similar in complexity, with the topsides often exposed to severe wind storms (in many cases tropical cyclones), as well as wave action. In these cases the overall wind forces on the above water-exposed structure is of interest in the design of the underwater foundations and supporting structure.

The low frequencies of 'compliant' offshore structures, such as tension leg or guyed structures in deep water locations, are of special concern because of the need to consider resonant excitation by dynamic wind forces. The frequencies of some structures of this type can be so low that they are near the peak of the spectrum of wind forces in synoptic winds (Section 3.3.4). However, it appears that hydrodynamic damping, resulting from the underwater motion of the structure (Cook *et al*., 1986), largely mitigates resonant effects. The special problems of wind effects on compliant offshore structures are discussed in a number of specialist publications (e.g. Smith and Simiu, 1986).

14.8 Summary

In this chapter, wind loads on structures not covered in Chapters 8 to 13, have been discussed. This category includes free-standing walls and hoardings, attachments to buildings such as canopies and awnings, and solar collectors.

Communications and broadcasting antennas of various types, particularly those impermeable enough to attract substantial wind loading, are considered in some detail. Some discussion of wind loads on elements in complex industrial structures such as oil refineries, and on offshore oil platforms has also been given.

References

British Standards Institution (1997) *Loading for Buildings. Part 2. Code of Practice for Wind Loads*. BS 6399: Part 2: 1997.

Cook, G. R., Kumarasena, T. and Simiu, E. (1986) Amplification of wind effects on compliant platforms. *Structures Congress '86*, New Orleans, September 15–18, (Proceedings of session: Wind effects on compliant offshore structures), A.S.C.E., New York.

E.S.D.U. (1981) Lattice structures Part 2 – Mean forces on tower-like space frames. Engineering Sciences Data Unit (ESDU International PLC, London, U.K.). ESDU Data Items 81028.

—— (1990), 'Structures of non-circular cross-section', Engineering Sciences Data Unit (ESDU International plc, London, U.K.). ESDU Data Items 90036.

Ginger, J. D. and Letchford, C. W. (1994) 'Wind loads on planar canopy roofs – Part 2: fluctuating pressure distributions and correlations', *Journal of Wind Engineering and Industrial Aerodynamics* 51: 353–70.

Gumley, S. J. (1984) 'A parametric study of extreme pressures for the static design of canopy structures', *Journal of Wind Engineering and Industrial Aerodynamics* 16: 43–56.

Holmes, J. D. (2000) 'Wind loading of parallel free-standing walls on bridges, cliffs and embankments', *4th International Colloquium on Bluff Body Aerodynamics and Applications*. Bochum, Germany, September 11–14.

Holmes, J. D., Banks, R. W. and Roberts, G. (1993) 'Drag and aerodynamic interference on microwave dish antennas and their supporting towers', *Journal of Wind Engineering and Industrial Aerodynamics* 50: 263–69.

Jancauskas, E. D. and Holmes, J. D. (1985) 'Wind loads on attached canopies', *Fifth U.S. National Conference on Wind Engineering*, Lubbock, Texas, U.S.A., November 6–8.

Kind, R. J. (1988) 'Worst suctions near edges of flat rooftops with parapets', *Journal of Wind Engineering and Industrial Aerodynamics* 31: 251–64.

Koss, L. L. and Melbourne, W. H. (1995) 'Chain dampers for control of wind-induced vibration of tower and mast structures', *Engineering Structures* 17: 622–5.

Letchford, C. W. and Ginger, J. D. (1992) 'Wind loads on planar canopy roofs – Part 1: mean pressure distributions', *Journal of Wind Engineering and Industrial Aerodynamics* 45: 25–45.

Letchford, C. W. and Holmes, J. D. (1994) 'Wind loads on free-standing walls in turbulent boundary layers', *Journal of Wind Engineering and Industrial Aerodynamics* 51: 1–27.

Lombardi, G. (1989) 'Wind-tunnel tests on a model antenna with different fin configurations', *Engineering Structures* 11: 134–8.

—— (1991) 'Wind-tunnel tests on a model antenna rotating in a cross flow', *Engineering Structures* 13: 345–50.

Marchman, J. F. and Werme, T. D. (1982) 'Mutual interference drag on signs and luminaires', *A.S.C.E. Journal of the Structural Division* 108: 2235–44.

Newton, J. R. H. (1983) 'Wind effects on buildings – recent studies at Redland wind tunnel', *Journal of Wind Engineering and Industrial Aerodynamics* 11: 175–86.

Robertson, A. P., Hoxey, R. P. and Moran, P. (1985) 'A full-scale study of wind loads on agricultural canopy roof ridged structures and proposals for design', *Journal of Wind Engineering and Industrial Aerodynamics* 21: 113–25.

Sachs, P. (1978) *Wind Forces in Engineering*. Oxford: Pergamon Press.

Smith, C. E. and Simiu, E. (eds). (1986) 'Wind effects on compliant offshore structures', *Proceedings of a session at Structures Congress '86*, New Orleans, September 15–18, New York: A.S.C.E.

Standards Australia (1989) *Minimum Design Loads on Structures. Part 2: Wind Loads*. Standards Australia, North Sydney, Australian Standard AS1170.2-1989.

Tieleman, H. W., Akins, R. E. and Sparks, P. R. (1980) 'An investigation on wind loads on solar collectors', Virginia Polytechnic Institute and State University, College of Engineering, Report VPI-E-80-1.

Wyatt, T. A. (1964) 'The aerodynamics of shallow paraboloid antennas', *Annals, New York Academy of Sciences* 116: 222–38.